



# 1 **ATAT 1.0, an Automated Timing Accordance Tool for** 2 **comparing ice-sheet model output with geochronological data**

3 Jeremy C. Ely<sup>1</sup>, Chris D. Clark<sup>1</sup>, David Small<sup>2</sup> and Richard C.A. Hindmarsh<sup>3</sup>

4 <sup>1</sup>Department of Geography, The University of Sheffield, Sheffield, S10 2TN, UK

5 <sup>2</sup>Department of Geography, Durham University, Durham, DH1 3LE, UK

6 <sup>3</sup>British Antarctic Survey, High Cross, Madingley Road, Cambridge, CB3 0ET, UK

7 *Correspondence to:* Jeremy C. Ely ([j.ely@sheffield.ac.uk](mailto:j.ely@sheffield.ac.uk))

8 **Abstract.** Earth's extant ice sheets are of great societal importance given their ongoing and potential future  
9 contributions to sea-level rise. Numerical models of ice sheets are designed to simulate ice sheet behaviour in  
10 response to climate changes, but to be improved require validation against observations. The direct  
11 observational record of extant ice sheets is limited to a few recent decades, but there is a large and growing body  
12 of geochronological evidence spanning millennia constraining the behaviour of palaeo-ice sheets. Hindcasts can  
13 be used to improve model formulations and study interactions between ice sheets, the climate system and  
14 landscape. However, ice-sheet modelling results have inherent quantitative errors stemming from parameter  
15 uncertainty and their internal dynamics, leading many modellers to perform ensemble simulations, while  
16 uncertainty in geochronological evidence necessitates expert interpretation. Quantitative tools are essential to  
17 examine which members of an ice-sheet model ensemble best fit the constraints provided by geochronological  
18 data. We present an Automated Timing Accordance Tool (ATAT version 1.0) used to quantify differences  
19 between model results and geo-data on the timing of ice sheet advance and/or retreat. To demonstrate its utility,  
20 we perform three simplified ice-sheet modelling experiments of the former British-Irish Ice Sheet. These  
21 illustrate how ATAT can be used to quantify model performance, either by using the discrete locations where  
22 the data originated together with dating constraints or by comparing model outputs with empirically-derived  
23 reconstructions that have used these data along with wider expert knowledge. The ATAT code is made available  
24 and can be used by ice-sheet modellers to quantify the goodness of fit of hindcasts. ATAT may also be useful  
25 for highlighting data inconsistent with glaciological principles or reconstructions that cannot be replicated by an  
26 ice sheet model.

## 27 **1 Introduction**

28 Numerical models have been developed which simulate ice sheets under a given climate forcing (e.g. Greve,  
29 1995; Rutt et al., 2009; Pollard and DeConto, 2009; Winkelmann et al., 2011; Gudmundsson et al., 2012;  
30 Cornford et al., 2013; Pattyn, 2017). When driven by future climate scenarios, these models are used to forecast  
31 the fate of the Antarctic and Greenland ice sheets (e.g. Seddik et al., 2012; DeConto and Pollard, 2016),  
32 providing predictions of their potential contribution to future sea level rise. However, incomplete knowledge of  
33 ice physics, boundary conditions (e.g. basal topography) and parameterisations of physical processes (e.g. basal  
34 sliding, calving), as well as the difficulty of predicting future climate, lead to uncertainty in these predictions  
35 (Applegate et al., 2012; Briggs et al., 2014; Ritz et al., 2015). Observations of ice marginal fluctuations  
36 (decades) and the processes of ice calving, flow or melting (subaerial or submarine) that facilitate or drive such



37 variations, provide a powerful means to understand the processes leading to the possibility of deriving new  
38 formulations that improve the realism of modelling. However, the short-time span (decades) of these  
39 observations limits their being used to constrain, initialise or validate modelling experiments (Bamber and  
40 Aspinall, 2013). Conversely, palaeo-ice sheets, especially from the last glaciation (~21,000 years ago), left  
41 behind evidence which provides the opportunity to study ice sheet variations across timescales of centuries to  
42 millennia, albeit with increased uncertainty in exact timing.

43 Numerous modelling studies have aimed to simulate the growth and decay of palaeo-ice sheets, producing  
44 hindcasts of ice-sheet behaviour (e.g. Boulton and Hagdorn, 2006; Hubbard et al., 2009; Tarasov et al., 2012;  
45 Gasson et al., 2016; Patton et al., 2016). Results from these hindcasts may be compared with empirical data  
46 recording ice sheet activity, so as to discern which parameter combinations produce results that best replicate the  
47 evidence of palaeo-ice sheet activity. Three classes of data are of particular use for constraining palaeo-ice  
48 sheets; (i) geomorphological data, (ii) relative sea level history, and (iii) geochronological data.

49 Geomorphological evidence comprises the landforms created by the action of ice upon the landscape, and can  
50 typically provide data on ice extent, recorded by moraines and other ice marginal landforms and on ice-flow  
51 directions recorded by subglacial landforms such as drumlins. Such landforms can be used to decipher the  
52 pattern of glaciation (e.g. Kleman et al., 2006; Clark et al., 2012; Hughes et al., 2014). Two tools have already  
53 been developed which can compare modelled ice margins and flow directions to the geomorphological evidence  
54 base (Napieralski et al., 2007).

55 Relative sea level data provides information regarding the mass-loading history of an ice sheet. Palaeo-ice-sheet  
56 model output is often evaluated against relative-sea-level data by use of glacio-isostatic adjustment models (e.g.  
57 Tushingham and Peltier, 1992; Simpson et al., 2009; Tarasov et al., 2012).

58 Geochronological evidence attempts to ascertain the absolute timing of ice advance and retreat using dated  
59 material (e.g. organic remains dated by radiocarbon measurement) found in sedimentary contexts interpreted as  
60 indicating ice presence or absence nearby. It enables reconstruction of the chronology of palaeo-ice sheet  
61 growth and decay (Small et al., 2017) and is the underpinning basis for empirically-based ice sheet margin  
62 reconstructions (e.g. Dyke, 2004; Clark et al., 2012; Hughes et al., 2016). Although widely used in empirical  
63 reconstruction of palaeo-ice sheets, geochronological data has rarely been directly compared with ice sheet  
64 model output (although see Briggs and Tarasov, 2013). Such a comparison could be useful both for constraining  
65 ice-sheet model uncertainty and for identifying problems with the geochronological record. For example, a poor  
66 fit between model output and empirical data on timing could inform on the validity of a numerical model (or its  
67 parameterisation), or it could provide a physical basis for questioning the plausibility of empirically-driven  
68 interpretations or specific lines/data points of evidence given that they are associated with inherent uncertainties.  
69 In order to maximise the benefit to all users, any comparisons between palaeo-ice sheet model output and  
70 empirical data should ideally consider the inherent uncertainties of both.

71 Given the wide availability of compilations of geochronological data (e.g. Dyke, 2004; Hughes et al., 2011;  
72 Hughes et al., 2016), as well as the proliferation of ice sheet models (e.g. Greve, 1995; Rutt et al., 2009; Pollard  
73 and DeConto, 2009; Winkelmann et al., 2011; Gudmundsson et al., 2012; Cornford et al., 2013; Pattyn, 2017), a  
74 convenient, reproducible and consistent procedure for comparison should be of great utility to the palaeo-ice  
75 sheet community. The typical volume of geochronological constraints (several thousands) for a palaeo ice sheet  
76 and the number of ensemble runs (several hundreds) from an ice sheet model make a visual matching of data



77 and model output nearly impossible to accomplish, which is likely to explain the rarity of such comparisons.  
78 Here, we present an Automated Timing Accordance Tool (ATAT, version 1.0) that compares geochronological  
79 data and ice-sheet model output. The tool is in the form of a Python script and requires the installation of open-  
80 source libraries. ATAT is written to handle NETCDF data as an input, a format commonly used in ice sheet  
81 modelling and is also accessible from many GIS packages in which geochronological data can be stored and  
82 manipulated.

## 83 **2 Background**

84 Geochronological evidence and ice sheet model outputs are often independently used to reconstruct the timing  
85 of glaciological events. The two approaches are fundamentally different in nature and consequently produce  
86 contrasting data outputs. Thus, before describing our approach to comparing the two sets of data (ATAT), we  
87 first consider the nature of both geochronological data and ice-sheet model output to highlight the issues and  
88 potential difficulties associated with comparing the two and conceptualise a comparison procedure.

### 89 **2.1 Geochronological data**

90 The timing of palaeo-ice sheet activity has primarily been dated using three techniques: (i) radiocarbon dating;  
91 (ii) cosmogenic nuclide exposure dating, and (iii) luminescence dating (Figure 1). The utility of each method for  
92 determining the timing of palaeo-ice sheet activity has been extensively reviewed elsewhere (e.g. Fuchs and  
93 Owen, 2008; Balco 2011; Small et al., 2017) and only a brief description is provided here. Radiocarbon dating  
94 uses the known rate of the radioactive decay of  $^{14}\text{C}$  to determine the time elapsed since the death of organic  
95 material (Libby et al., 1949; Arnold and Libby, 1951; Figure 1). For palaeo-glaciological purposes, the dated  
96 organic material (e.g. shells, mosses, plant remains) is usually taken from basal sediments overlying and closely  
97 associated with a glacial deposit in order to determine a minimum deglaciation age (e.g. Heroy and Anderson,  
98 2007; Lowell et al., 2009); ice is interpreted to have retreated from this site some short time prior to this age.  
99 Where organic matter is either reworked within or is located directly beneath a glacial deposit, it can be used to  
100 constrain the maximum age of glacial advance (e.g. Brown et al., 2007; Ó Cofaigh and Evans, 2007); advance  
101 happened sometime after this age. Cosmogenic nuclides (e.g.  $^{10}\text{Be}$ ,  $^{26}\text{Al}$  and  $^{36}\text{Cl}$ ) are produced by the  
102 interaction of secondary cosmic radiation in minerals, such as quartz, within materials exposed at the Earth's  
103 surface (Figure 1). Samples are generally taken from glacially-transported boulders, morainic boulders and  
104 glacially modified bedrock, all of which have ideally had signals from any previous exposure history removed  
105 by glacial erosion. Cosmogenic nuclide dating is thus used to determine the duration of time a sample has been  
106 exposed at the Earth's surface by determination of the concentration of cosmogenic nuclides within that sample.  
107 Luminescence dating can determine the age of a deposit by measuring the charge accumulated within minerals.  
108 This charge accumulates in light-sensitive traps within the crystal lattice due to ionizing radiation produced by  
109 naturally occurring radioactive elements (e.g. U, Th, K). Luminescence dating determines the time elapsed since  
110 the last exposure of the mineral to sunlight; this exposure acts to reset the signal (Figure 1). As subglacial  
111 deposits are unlikely to have been exposed to light before burial, and therefore contain signals accumulated prior  
112 to deposition, luminescence dating within palaeo-glaciology is typically applied to ice marginal sediments, or  
113 those which overly glacial sediments (e.g. Duller, 2006; Smedley et al., 2016; Bateman et al., 2018). All



114 geochronological techniques record the absence of grounded ice. They therefore provide either maximum or  
115 minimum ages of a glaciological event, depending upon the stratigraphic setting. Table 1 outlines a commonly  
116 used system used to classify geochronological data by stratigraphic setting (Hughes et al., 2011; 2016).

117 The retreat/advance (ice-free) ages provided by the three geochronometric techniques are all affected by  
118 systematic and geological uncertainties (Small et al., 2017). Systematic uncertainties originate from the tools  
119 and techniques used to derive the date, such as laboratory instruments and sample preparation, and are  
120 accounted for in the quoted errors that accompany a date. Geological uncertainties are caused by the geological  
121 history of a sample, before, during and after a glacial event (e.g. Lowe and Walker, 2000; Lukas et al., 2007;  
122 Heyman et al., 2011). Such influences may leave little or no evidence of their effect upon a sample and are thus  
123 hard to quantify. The relationship between a dated sample and the glacial event it indicates is the largest  
124 potential source of uncertainty in geochronological data and is primarily bounded by the ability of the  
125 investigator to find and associate dateable material to the glacial event of interest. Since all geochronological  
126 techniques measure the absence of ice, expert inference must be made, and are influenced by the availability of  
127 information (stratigraphic or otherwise) at a study site; they may be open to change (e.g. new radiocarbon  
128 calibrations, new cosmogenic isotope production rates). Furthermore, in the cases of luminescence and  
129 radiocarbon dating, there can be an unknown duration since glacial occupation of an area and the deposition of  
130 dateable material. These factors mean it is necessary to consider the quality of dates for ascertaining the timing  
131 of the glacial event in question (Small et al., 2017).

132 Numerous geochronological studies have sought to ascertain the timing of palaeo-ice sheet activity at sites,  
133 leading to compilations of geochronological data which bring together hundreds to thousands of published dates  
134 (e.g. Dyke et al., 2002; Livingstone et al., 2012; Hughes et al., 2011; 2016). Despite the growing number of  
135 reported dates, they are still insufficient in number and spatial spread to define, on their own, the time-space  
136 envelope of the shrinking ice sheet. Techniques to interpolate geochronological information between sites are  
137 required. The most commonly used technique is empirical ice sheet reconstruction (e.g. Dyke, 2004; Clark et al.,  
138 2012), whereby expert assessments of the geochronological and geomorphological record are used together to  
139 create ice-sheet wide isochrones of ice-sheet margin position and flow configuration. A recent advance in this  
140 method has been the inclusion of confidence envelopes for each isochrone, documenting possible maximum,  
141 likely and minimum extents (Hughes et al., 2016). Further techniques for spatiotemporally interpolating  
142 geochronological data include Bayesian sequence modelling (e.g. Chiverrell et al., 2013; Smedley et al., 2017),  
143 in which collections of deglacial ages are arranged in spatial order determined by a priori knowledge of  
144 geomorphologically-informed ice flow and retreat patterns (e.g. Gowan, 2013). Such techniques provide viable  
145 methods for producing ice-sheet wide chronologies, filling in information in locations where geochronological  
146 data may be sparse.

## 147 **2.2 Ice sheet model output**

148 Ice-sheet models solve equations for ice flow over a computational domain, for a given set of input parameters  
149 and boundary conditions, to determine the likely flow geometry and extent of an ice sheet. Typically, ice-sheet  
150 models run using finite difference techniques on regular grids (e.g. Rutt et al., 2009; Winkelmann et al., 2011).  
151 Ice-sheet models that utilise adaptive meshes (e.g. Cornford et al., 2013) and unstructured meshes also exist  
152 (e.g. Larour et al., 2012) and the results from such models can be interpolated onto spatially regular grids. The



153 spatial resolution of an ice-sheet model depends upon the computational resources available, and the spatial  
154 resolution of available boundary conditions. Continental-scale models of palaeo-ice sheets have typical spatial  
155 resolution of tens of kilometres (e.g. Briggs and Tarasov, 2013; DeConto and Pollard, 2016; Patton et al., 2016),  
156 though parallel, high-performance computing means higher resolutions are possible (e.g. 5 km in Golledge et  
157 al., 2013 and Seguinot et al., 2016). The temporal resolution of ice sheet model output is ultimately limited by  
158 the time-steps imposed by the stability properties of the numerical schemes solving the ice-flow equations.  
159 Given that these stable time-steps can be sub-annual, output frequency is mostly predetermined by the user  
160 (typically decades to centuries), and as such is constrained by available disk-storage. Ice-sheet models therefore  
161 produce spatially connected predictions of ice-sheet behaviour such as advance and deglaciation (e.g. Table 1)  
162 across gridded domains at various temporal and spatial resolutions.

163 The stress fields imposed upon ice can be fully described by solving the Stokes equations. Indeed, ‘full Stokes’  
164 models which do so have been tested (Pattyn et al., 2008) and used to simulate ice sheets (e.g. Seddik et al.,  
165 2012). However, fully solving the Stokes equations over the spatio-temporal scales relevant to palaeo-ice sheet  
166 researchers remains beyond the limit of currently available computational power. This problem is exacerbated  
167 by the need to run multi-parameter valued ensemble simulations to account for model uncertainty over multi-  
168 millennial and continental-scale domains. This means that palaeo-ice sheet modelling experiments rely upon  
169 approximations of the Stokes equations (see Kirchner et al., 2011 for a discussion), such as the shallow ice  
170 approximation (SIA) and shallow shelf approximation (SSA). The choice of ice-flow approximation used within  
171 a model has implications for the capability of models to realistically capture aspects of ice sheet flow  
172 (Hindmarsh, 2009; Kirchner et al., 2011; 2016), and in turn influences the nature of the model output produced.  
173 For instance, the SIA is not applicable for ice shelves, therefore SIA-based models do not produce modelled ice  
174 shelves (e.g. Glimmer; Rutt et al., 2009). Therefore, the timing of deglaciation in an SIA model can be  
175 determined as the point at which ice thickness in a cell becomes zero or thinner than the flotation thickness. In a  
176 model which predicts the location of ice shelves (e.g. a SSA or higher-order model), the location and movement  
177 of the grounding line must be determined in order to calculate the modelled retreat or advance age. Such models  
178 typically produce a ‘mask’ variable from which the extent of grounded ice can be determined (e.g. PISM;  
179 Winkelmann et al., 2011).

180 Though ice sheet models produce output which is consistent with model physics, there are many sources of  
181 uncertainty involved with ice sheet modelling. This uncertainty has two main sources: (i) parameterisations, and  
182 (ii) boundary conditions. Where a process is too complex (e.g. calving) or occurs at too small a scale (e.g.  
183 regelation) to be captured by an ice sheet model, it is often simplified and parameterised. Associated with each  
184 parameterisation are a set of parameters, the values of which are either unknown, or thought to vary within some  
185 plausible bounds. This leads to an associated uncertainty when choosing these input parameters, which can  
186 either be constant or spatially and temporally variable across a domain. An example of a process which is often  
187 parameterised is basal sliding. This parameterisation is often done through the implementation of a sliding law  
188 (e.g. Fowler, 1986; Bueler and Brown, 2009; Schoof, 2010), which relates the basal shear stress to the basal  
189 velocity (Fowler, 1986). Exact determination of basal shear stress requires knowledge of basal roughness,  
190 hydrological conditions and, where present, sediment rheology. These terms are often assigned or incorporated  
191 within a parameter, or prescribed by another model parameterisation (e.g. a subglacial hydrology model).



192 Adding to the uncertainty in the absence of a single preferable sliding law, ice-sheet models often allow the user  
193 to choose between different sliding law implementations.

194 Boundary conditions, the values prescribed at the edge of the modelled domain, also introduce uncertainty into  
195 ice-sheet models. For contemporary ice sheets, there is a large uncertainty in the basal topography (e.g. Fretwell  
196 et al., 2013). This is less of a problem for the more accessible beds of palaeo-ice sheets. However, accurately  
197 accounting for the evolution of this bed topography over the course of a glaciation requires a model of isostatic  
198 adjustment (Lingle and Clark, 1985; Gomez et al., 2013).

199 A very large source of uncertainty for modelling palaeo-ice sheets is the climate used to drive them (Stokes et  
200 al., 2015), as indeed is the case for forecasts of contemporary ice sheets (e.g. Edwards et al., 2014). Owing to  
201 the computational resources required and technical challenges, few palaeo-ice sheet models are coupled with  
202 climate models. Palaeo-ice sheet modellers have mostly used offline methods to force their models with  
203 representations of palaeo-climate. These include simple parameterisations (Boulton and Hagdorn, 2006),  
204 applying offsets derived from ice core records to contemporary climate (Hubbard et al., 2009) and scaling  
205 between present-day conditions and uncoupled global-circulation-model simulations at maximum glacial  
206 conditions (Gregoire et al., 2012; Gasson et al., 2016). Each approach has advantages and disadvantages, but,  
207 most importantly, is also associated with an inherent uncertainty. When this uncertainty is accounted for, the  
208 range of possible climates produces numerous ice sheet outputs.

209 There is another cause of ice-sheet models not being able to accurately predict the evolution of ice-sheets, which  
210 is the presence of instabilities – we use this term in the technical sense of a small perturbation in leads to the  
211 whole ice-sheet system amplifying this small perturbation to the extent it can leave a mark in the geological  
212 record. A classic example of this in ice-sheet dynamics is the marine ice-sheet instability (MISI), first discussed  
213 in the 1970s (Hughes, 1973; Weertman, 1974, Mercer, 1978) and more recently put on a sounder mathematical  
214 footing (Schoof 2007, 2012).

215 The MISI actually refers to an instability in grounding-line (GL) position on a reverse slope, where the water  
216 depth is shallowing in the direction of ice flow. Since ice flux increases with ice thickness, a straightforward  
217 argument leads to the conclusion that if the GL advances into shallower water, the efflux will decrease, the ice  
218 sheet will gain mass and the advance continue. If, on the other hand, the GL retreats, the efflux will increase, the  
219 ice-sheet will lose mass and the retreat continue. The latter process led to concerns that the retreat of Antarctic  
220 and Greenlandic ice-sheets would cause several metres of sea-level rise over one or two centuries. Schoof  
221 (2007,2012) showed that the MISI was in accordance with the understanding and use of the word ‘instability’ by  
222 physicists and mathematicians.

223 In principle, given the right parameterisations and basal topography, ice-sheet models should be able to predict  
224 the ‘trajectory’ of GL migration arising as a consequence of the MISI. However, the MISI is one of the class of  
225 instabilities that lead to poor predictability; certain small variations of parameters and specifications will lead to  
226 large-scale changes in the ‘trajectory’, in this case the retreat history. A well-known analogy is the ‘butterfly  
227 effect’, which originated in atmospheric modelling work (Lorenz, 1963); the butterfly effect is concerned with  
228 the consequences of the statement “small causes can have larger effects”.

229 Schoof’s theory was for a very straightforward marine ice-sheet configuration – no buttressing, ice motion all by  
230 sliding, isothermal, but its accuracy was confirmed by a large group of researchers running their models for this  
231 simple configuration (Pattyn et al., 2012). Schoof (2012) showed that for his configuration, the existence of a



232 reverse slope was sufficient condition for the MISI to exist. However, later work (Gudmundsson, 2012; Gomez  
233 et al., 2012) presented results showing that stable GL positions could exist on a reverse slope if extra physical  
234 processes were included (Gudmundsson introduced buttressing, Gomez et al. included the effect of lateral  
235 gravitational attraction on sea-level). Their results indicated that the reverse slope was not a sufficient condition  
236 for instability.

237 Most of the palaeo-ice sheets at the LGM had extensive marine margins at their polar edges, certainly the  
238 Laurentide, Fennoscandian and British-Irish ice-sheets, and the present-day bathymetry of the seas around North  
239 America and Europe strongly suggests that a reverse-slope would have existed – moreover, isostatic adjustment  
240 under the weight of the ice-sheets would have created further extensive zones of reverse slope. There are data  
241 indicating rapid retreat along some zones of reverse slope in palaeo-ice sheets, which leads to the question of  
242 how accurately we should expect ice-sheet models to be able to reproduce the observed retreat rates in the  
243 presence of physical instability. Schoof's progress is very recent, so the necessary ensemble runs have yet to be  
244 carried out by researchers focussing on the relationship between the presence of the MISI and the amplification  
245 of data uncertainties or physics errors/over-simplifications (as placed in the models).

### 246 **2.3 Considerations when comparing geochronological data and ice-sheet model output**

247 Sections 2.1 and 2.2 make it clear that several factors must be considered in order to satisfactorily compare  
248 geochronological data and ice-sheet model output (Table 2). Most critically, the two datasets involved in any  
249 comparison have varying spatial properties. Raw geochronological data is unevenly distributed and located at  
250 specific points, with horizontal position accurate to a metre or so; such data may be used to plot ice-margin  
251 fluctuations of the order of tens of kilometres (Figure 2C). Ice-sheet models typically produce results on evenly-  
252 spaced points (at ~5 km to 20 km resolution) that are distributed over and beyond the maximum area of the  
253 palaeo-ice sheet (Table 2; Figure 2B). Consequently, in comparing the two, a choice must be made; either  
254 geochronological data should be gridded (coarsened) to the resolution of the ice-sheet model, or the ice-sheet  
255 model results must be interpolated to a higher resolution. Both options have drawbacks, as the former removes  
256 spatial accuracy from geochronological data while the latter relies upon interpolation beyond model resolution  
257 and, more seriously, model physics. A second problem lies in the spatial organisation of the data (Table 2). Ice-  
258 sheet models produce a regular grid of data (Figure 2B), meaning that no location is more significant than any  
259 other when comparing the modelled deglacial chronology with that inferred from geological data. Conversely,  
260 owing to the uneven distribution of raw geochronological data, some regions of a palaeo-ice sheet may be better  
261 constrained than others (Figure 2C). As noted by Briggs and Tarasov (2013), any comparison that does not treat  
262 the uneven spatial distribution of geochronological data may favour sites where numerous dates exist over more  
263 isolated locations. One approach to overcoming these disparities is to use an interpolation scheme (e.g.  
264 empirical reconstruction, Bayesian sequence) on the raw geochronological data. This produces a  
265 geochronological framework by combining evidence on pattern and timing to yield a distribution that is spatially  
266 more uniform and a spatial resolution similar to that of palaeo-ice sheet model output (Figure 2D).

267 The temporal intervals between and precision of geochronological data and ice sheet model output also vary  
268 (Table 2). The time intervals between geochronometric data are determined by the number of available  
269 observations, and precision determined by sources of uncertainty. Conversely, ice sheet models produce output  
270 at regular intervals and are temporally exact, which is to be contrasted with 'correct'. Since the output interval



271 of an ice-sheet model is generally determined by the user (see Section 2.2) it is pertinent to consider an  
272 appropriate time-interval of ice-sheet model output for comparison with geochronological data. For example,  
273 radiocarbon dates have precision typically in the order of hundreds of years but do not directly constrain ice  
274 extent, whilst empirically reconstructed isochrones are typically produced for thousand-year time-slices (e.g.  
275 Hughes et al., 2016). In reality, ice sheets may respond to events at faster time-scales than this, but in the  
276 absence of internal instabilities (e.g. MISI) palaeo-ice sheet models are ultimately limited by the temporal  
277 resolution of the available climate forcing data. Thus, to gain insight into controls on palaeo-ice sheet behaviour,  
278 it may be necessary to create model output with a greater (centurial) temporal resolution than the uncertainty  
279 associated with geochronology.

280 Both geochronological data and ice-sheet model output have sources of uncertainty which must also be  
281 considered when comparing the two. For geochronological data, uncertainty is typically expressed as a standard  
282 deviation from the reported age, and are therefore easy to consider when comparing to an ice sheet model. For  
283 ice-sheet models, individual model runs do not currently express uncertainty, and it is only when multiple,  
284 ensemble, runs which systematically vary parameters and boundary conditions are conducted that uncertainty in  
285 all output variables can be expressed. Having said this, statistical techniques exist to derive probability  
286 distribution functions for individual quantities (e.g. Ritz et al., 2015). Such ensemble runs typical comprise  
287 hundreds to thousands of individual runs (Tarasov and Peltier, 2004; Robinson et al., 2011). Given the volume  
288 of data this produces, one appealing application of a quantitative comparison between geochronological data and  
289 ice sheet model output would be to act as a filter for scoring ice-sheet model runs and reducing predictive  
290 uncertainty by only using the parameter combinations that were successful. However, if all possible parameters  
291 have been modelled, (i.e. the full ‘phase-space’ of the model has been explored (cf. Briggs and Tarasov, 2013)),  
292 and very few (or no) model runs conform to a certain set of geochronological data or an empirical  
293 reconstruction, this may provide a basis to question aspects of the evidence (e.g. re-examining the stratigraphic  
294 context of a dated sample site or questioning the basis of the reconstructed isochrone). Of course, a third  
295 possibility that both data and model are incorrect cannot be excluded.

296 We therefore suggest that any comparison between ice-sheet model experiments and geochronological data  
297 should consider:

- 298 i) That both ice-sheet models and geochronological data have inherent uncertainties;
- 299 ii) That geochronological data typically provide a constraint on just the absence of ice; such that ice must have  
300 withdrawn from a site sometime (50 years? 500 years? 5000 years?) prior to the date (which can be any point  
301 within the full range of the stated uncertainty). It thus a limit in time and not a direct fix. Figure 3 illustrates this  
302 for advance and retreat constraints. It is most often the case that dated material is taken close to the stratigraphic  
303 boundary or landform representing ice presence, in which case a date might be considered as a ‘tight constraint’  
304 (e.g. the ice withdrew and very soon afterwards (50 years) marine fauna colonised the area and deposited the  
305 shells used in dating). Sometimes however there may have been a large (centuries to millennia) interval of time  
306 between the withdrawal and the age of the shell chosen as a sample, in which case the date will provide a ‘loose’  
307 limiting constraint; it might be much younger than ice retreat (Figure 3).
- 308 iii) There is inherent value to the expert interpretation of stratigraphic and geomorphological information,  
309 meaning an ice-free age reported for a site is likely as close as possible (tight constraint) to a glacial event.  
310 However, this interpretation could be subject to change;





311 iv) Geochronological data exist as spatially distributed dated sites (e.g. Figure 2C) which can be built into a  
312 spatially coherent reconstruction (e.g. Figure 2D);  
313 v) A great input uncertainty in a palaeo-ice sheet model is the climate, which can lead to changes in the spatial  
314 extent and timing of ice sheet activity.  
315 vi) A factor which requires further investigation is the relationship between the operation of a physical  
316 instability (e.g. the MISI) and the practical ability of models to predict retreat or advance rates; the presence of  
317 an instability can result in extreme sensitivity to parameter ignorance or over-simplified model physics.  
318 vii) Other uncertainties can also lead to variations in ice-sheet model results; these can be accounted for in an  
319 ensemble of hundreds to thousands of simulations.  
320 Given the above, it is unlikely that a single procedure could capture model-data conformity. ATAT therefore  
321 implements several ways of measuring data-model discrepancies and produces output maps (described in the  
322 following two sections) to help a user assess which model runs best agree with the available geochronological  
323 data. One approach is to transform the geochronological data points (x,y,t) to a gridded field (raster) that define  
324 age constraints of ice advance and another grid for retreat. Both of these data types also require an associated  
325 grid that reports the uncertainty range as error (Figure 4). These age grids may then be quantitatively compared  
326 to equivalent grids (age of advance grid and age of retreat grid) derived from the ice sheet model outputs.  
327 Alternatively, one might prefer to compare model runs against the geochronological data (points) combined with  
328 expert-sourced interpretive geomorphological and geological data, in which age constraints from dated sites  
329 have been spatially extrapolated using moraines and the wider retreat pattern. In this case ATAT allows the  
330 model outputs to be compared to the ‘lines on maps’ type of reconstruction subsequent to conversion from age  
331 isolines to a grid of ages (Figure 4).

### 332 **3. Description of tool**

333 ATAT is written in Python, and utilises several freely available modules. Access to these modules may require a  
334 Python package manager, such as ‘pip’ or ‘anaconda’. ATAT can therefore be run from the command line on  
335 any operating system, or by using a Python interface such as IDLE.

#### 336 **3.1 Required data and processing**

337 ATAT requires two datasets as an input: (i) an ice-sheet model output; and (ii) gridded geochronological data.  
338 Table 3 provides the required variables and standard names for each dataset. In order to determine the advance  
339 age or deglacial age predicted by the ice sheet model, ATAT requires either an ice thickness (where the model  
340 does not produce ice shelves) or a grounded ice-mask variable (where ice shelves are modelled). In the latter  
341 case, the user is asked to define the value which represents grounded ice.  
342 Empirical advance and deglacial geochronological data (Table 1) require separate input files (NETCDF format),  
343 as model-data comparison for these two scenarios are run separately in ATAT. Table 1 and further references  
344 (Hughes et al., 2011; 2016; Small et al., 2017), provide information regarding identification of the stratigraphic  
345 setting of these two glaciological events as considered by ATAT. ATAT requires that geochronological data  
346 (advance or deglacial) are interpolated onto the same grid projection and resolution as the ice-sheet model  
347 before use. Though an imperfect solution to the problem of comparing grids of different resolution, (Section 2.3;



348 Table 2), this was preferred to the alternative solution of regriding an ice sheet model onto a higher resolution  
349 grid, as this may introduce the false impression of high resolution modelling sensitive to boundary conditions  
350 (e.g. topography) beyond the actual model resolution.

351 Preparation of the geochronological data to be the same format and grid resolution as the ice sheet model output  
352 requires use of a GIS software package such as ESRI ArcMap or QGIS. Users must define deglacial/advance  
353 ages based either upon the availability of geochronological data in a cell, or based upon an empirical  
354 reconstruction (Figure 4). Where there are no data (i.e. outside the ice-sheet limit), the grid value must be kept at  
355 0. Given that this may involve many expert decisions (e.g. which date has the relevant stratigraphic setting,  
356 which date(s) are most reliable?), this part of the process is not yet automated within ATAT. This data  
357 preparation stage is therefore the most time-consuming and user-intensive part of the process. However, users  
358 only need to define the data-based advance/deglacial grid once to compare to multiple model outputs.

359 Upon starting ATAT, the user is first asked to define whether they are testing a deglacial or advance scenario  
360 (Table 1; Figure 5). ATAT on considers the last time that ice advances over an area. Therefore, caution must be  
361 undertaken when defining advance data in regions where multiple readvances occur, and users should consider  
362 limiting the time interval of the ice sheet model tested when examining specific events (e.g. a well-dated  
363 readvance or ice sheet build-up). The location of the file containing the geochronological data grid (e.g. Figure  
364 5) is then required. From this file, the age and error grids are converted to arrays. For the age data, null values  
365 are masked out using the numpys masked array function. A second array that accounts for error is then created,  
366 the properties of which depends upon whether a deglacial or advance scenario is being tested. For a deglacial  
367 scenario, a model prediction will be unacceptable if the cell is ice-covered after the range of the date error is  
368 accounted for, but the cell may become deglacial any time before this. Therefore, the associated error value is  
369 added onto the cell date, to create a maximum age at which a cell must be deglacial by to conform to the ice  
370 sheet model (Figure 3). The opposite is true for advance ages; ice can cover a cell any time after the date and  
371 associated error, but cannot cover the cell before the date of the advance. In order to allow for advances which  
372 occur after the date and its error, associated error is therefore subtracted from the date cell (Figure 3). To  
373 account for the uneven spatial distribution of dates, a weighting for each date is then calculated based upon their  
374 spatial proximity. This weighting is used later when comparing the data to the model output. To calculate this  
375 weighting, the Euclidian distance from each dated cell to its nearest dated cell ( $d_i$ ) is calculated. The mean  
376 distance between dated cells ( $\bar{d}$ ) is then calculated, and the weight of each location ( $w_i$ ) defined using Eq. (1):

$$377 \quad w_i = \sqrt{\frac{d_i}{\bar{d}}},$$

378 (1)

379 The user is then asked to define the path to the ice sheet model output, from which the modelled deglacial age  
380 will be calculated and eventually compared to the data (Figure 4). The user is also asked whether to base  
381 deglacial timing on an ice thickness or grounded extent mask variable (Table 2). If the user selects thickness, the  
382 margin is defined by an increase from 0 ice thickness. For the mask, the user is also asked to supply the number  
383 which refers to grounded ice extent. The timing of advance is then determined by the change of a cell to this  
384 number (Figure 5).



### 385 3.2 Model-data comparison

386 Once the required variables have been retrieved from the NETCDF data and manipulated, ATAT compares the  
 387 geochronological age and modelled age at each location (Figure 4). Firstly, the grid cells which have data are  
 388 categorised as to whether there is model-data agreement, based on the criteria shown in Figure 3. Since all  
 389 dating techniques only record the absence of ice, geochronological data provides only a one-way constraint on  
 390 palaeo-ice sheet activity. For deglacial ages, deglaciation could occur any time before the geochronological data  
 391 provided and within the error of the date, but deglaciation must not occur after the error of the date is considered  
 392 (Figure 3). For advance ages, advance must have happened after the date or within error beforehand, but palaeo-  
 393 ice sheet advance cannot occur in the time period before that dated error (Figure 3). Once ATAT has determined  
 394 whether each cell conforms to these criteria, a map is produced identifying at which locations the ice sheet  
 395 model agrees with the geochronological data.

396 Though the criteria described above and illustrated in Figure 3 allow for the identification of dates which  
 397 conform to the predictions of an ice sheet model, they provide little insight into how close the timing of the  
 398 model prediction is to the geochronological data. If these were the only criteria on which a model-data  
 399 comparison was made, it could prove problematic. In an extreme case, one could envisage that all retreat dates  
 400 are adhered to by a model run that deglaciates from a maximum extent implausibly rapidly (say 50 years!), and,  
 401 given that we only have one-way constraints on deglaciation (Figure 3), this model run would conform to all  
 402 modelled dates. Whilst the nature of geochronological data (being only able to determine the absence of ice)  
 403 does not preclude such a scenario, this assumes that there is no inherent value to the expert judgement and  
 404 stratigraphic interpretation of each date as being close to palaeo-ice sheet timing (cf. Small et al. 2017).  
 405 Therefore, ATAT also determines the temporal proximity of the geochronological data and the model  
 406 prediction. Firstly, a map of the difference between modelled and empirical ages is created (Figure 5). This  
 407 enables the identification of dates which are a large distance away from the model prediction. Secondly, the  
 408 route-mean square error (RMSE) is calculated using the Eq. (2):

$$409 \quad RMSE = \sqrt{\frac{1}{n} \sum_{i=1}^n (g_i - m_i)^2},$$

410 (2)

411 where  $n$  is the number of cells which contain empirical geochronological information,  $g_i$  is the associated  
 412 geochronological date, and  $m_i$  is the model predicted age. The RMSE works well when the geochronological  
 413 data is evenly spatially distributed, either from a reconstruction (i.e. isochrones) or a wealth of dates. ATAT also  
 414 calculates a weighted RMSE (wRMSE), for situations where this is not the case (i.e. there is a paucity of dates  
 415 that are not distributed evenly across the domain) using Eq. (3):

$$416 \quad wRMSE = \sqrt{\frac{1}{n} \sum_{i=1}^n ((g_i - m_i) * w_i)^2},$$

417 (3)

418 where  $w_i$  is the spatial weighting factor determined in Eq. (1). Both the RMSE and wRMSE are calculated for  
 419 dated regions which have different levels of conformity with the model output (Figure 5). ATAT then produces  
 420 a .csv file with these statistics. Given the complexity of data-model comparison, different statistics may have



421 different uses. For instance, the percentage of covered dates may prove useful as a first filter of model runs,  
422 whilst the wRMSE of dates within error may be more convenient for choosing between filtered model runs.

#### 423 **4. Application of tool**

##### 424 **4.1 Ice Sheet Model**

425 To trial ATAT we used geochronological data and ice sheet modelling experiments from the former British-Irish  
426 Ice Sheet (BIIS). A vast quantity of previous research has produced a high density of dates (Hughes et al., 2011)  
427 which are being substantially augmented by the BRITICE-CHRONO project ([http://www.britice-  
428 chronology.group.shef.ac.uk/](http://www.britice-chronology.group.shef.ac.uk/)). Along with an abundance of well documented landforms (Clark et al., 2017), this  
429 makes the BIIS a data-rich study area for empirical reconstructions and ice sheet modelling. Ongoing modelling  
430 work aims to capture the behaviour of the BIIS inferred from the geomorphological and geochronological record  
431 (see Clark et al., 2012 for a recent reconstruction). We do not expect our model to capture these specific details.  
432 Instead, the purpose of modelling in this paper is merely to illustrate the use of ATAT. We therefore restrict  
433 ourselves to simplified modelling experiments and show only three model runs (Experiments A, B and C),  
434 whereas a full ensemble experiment would contain hundreds or thousands of simulations.

435 Ice sheet modelling experiments were conducted using the Parallel Ice Sheet Model (PISM; Winkelmann et al.,  
436 2011). This is a hybrid SIA-SSA model, with an implementation of grounding line physics. It is therefore suited  
437 to modelling both the marine-based portions of the BIIS and the terrestrial realm. The model simulates the  
438 history of the BIIS from 40 ka to present. The model is run at 5 km resolution, with basal topography derived  
439 from the General Bathymetric chart of the Oceans ([www.gebco.net](http://www.gebco.net)). This is updated to account for isostatic  
440 adjustment using a viscoelastic Earth model (Bueler et al., 2007) and a scalar eustatic sea level offset based on  
441 the SPECMAP data (Imbrie et al., 1984). All three model runs, labelled A-C, had the same input parameters and  
442 boundary conditions, apart from climate forcing. We take a similar approach to Seguinot et al. (2016) in  
443 computing a climate forcing. Modern values of temperature and precipitation are perturbed by a proxy  
444 temperature record, in this case the GRIP ice core record (Johnsen et al., 1995). These are input into a positive  
445 degree day model to calculate mass balance (Calov and Greve, 2005). Input precipitation values are the same  
446 between experiments. To introduce variation between the experiments, temperature varies such that Experiment  
447 A is the equivalent of modern day values, Experiment B has values uniformly reduced by 1°C and Experiment  
448 C has values uniformly reduced by 2°C. All other parameters and forcings are equal between experiments.

449 The maximum extent of ice for each experiment is shown in Figure 6 and the timing of advance and retreat is  
450 shown in Figure 7. Potentially unrealistic ice sheets occur in the North Sea, perhaps due to the choice of domain  
451 not including the influence of the Fennoscandian ice sheet in this area. As noted above, we do not expect these  
452 model runs to fully replicate the reconstructed characteristics of the BIIS (e.g. Clark et al., 2012). However, it is  
453 worth noting general, visually-derived, observations regarding the outputs shown in Figure 6. For larger  
454 temperature offsets, the ice sheet gets bigger, the timing of maximum extent gets progressively later and the  
455 modelled ice sheet gets thicker (Figure 6). In all experiments, there is generally a gradual advance toward the  
456 maximum extent followed by retreat (Figure 7). This pattern is interrupted by a later readvance that corresponds  
457 to the timing of the Younger Dryas in the GRIP record; this causes ice to regrow over high elevation areas such



458 as Scotland and central Wales. The extent of this readvance increases with decreased temperature offsets  
459 between experiments (Figure 7). Smaller readvances, occurring around 16.5 ka also occur (Figure 7).

#### 460 **4.2 Geochronological data**

461 Ice-sheet advance dates were taken from the compilation of Hughes et al. (2016) and gridded to the ice sheet  
462 model domain (Figure 4). In total, 61 cells were represented with advance dates (Figure 8A). Considering now  
463 ice-sheet retreat (Figure 8B), dates deemed reliable or probably reliable by Small et al. (2017) were used (i.e.  
464 those given a ‘traffic light rating’ of green or amber). For the dated advance and retreat locations, the  
465 geochronological data in each cell was assigned an error corresponding to that which was reported in the  
466 literature. We also compared our results to the ‘likely’ empirical reconstruction of Hughes et al. (2016), based  
467 on that of Clark et al. (2012) (Figure 8C), using the minimum and maximum bounding envelopes to assign an  
468 error to each cell of the ice sheet grid (Figure 8D). The largest errors occur in the North Sea region, where there  
469 is a lack of empirical data (e.g. Figures 8A and B).

#### 470 **4.3 Results**

471 Table 4 shows selected statistics derived by ATAT when comparing the three ice-sheet modelling experiments  
472 (Figures 6 and 7) against the three categories of data (Advance, Retreat, Isochrones; Figure 8). wRMSE was not  
473 calculated for the DATED isochrone reconstruction, as grid points are distributed evenly and therefore have  
474 equal spatial weighting (Table 4). Experiment C produces modelled ice-sheets with the greatest areal extent, and  
475 therefore performs best at correctly covering the dated areas (Table 4). However, none of the three experiments  
476 perform particularly well when compared with the data or the empirical reconstruction regarding timing and  
477 results in high (>2000 year) RMSEs (Table 4). The application of ATAT and the results from these simplified  
478 experiments allow us to suggest directions for analysing future experiments.

479 All three experiments produced large RMSEs, in the order of thousands of years, when compared to all three  
480 categories of data (Table 4). For advance ages, the three simulations conform to a large number of dated  
481 locations (e.g. 72% of ages in Experiments B and C; Table 4). However, the RMSEs of advance ages are high  
482 (Table 4). This shows that, while the models perform well at matching the constraint of covering an area in ice  
483 after an advance age (Figure 3), the models often glaciates a region much later than required. Advance dates are  
484 particularly difficult to obtain from the stratigraphic record, and often there may be a long hiatus between the  
485 initial deposition of datable material and the subsequent advance of a glacier. Future experiments with large  
486 ensembles should therefore consider the number of advance dates conformed to (rather than the RMSE) as a  
487 more robust guide for model performance during ice advance.

488 For the retreat comparisons, the three modelling experiments conform to a larger percentage of sites, seemingly  
489 outperforming the empirically-derived DATED reconstruction (Table 4). However, where model-data  
490 agreement occurs, the RMSE produced are much higher when for the model is compared to the DATED  
491 reconstruction. This is due to the reconstruction containing large uncertainties in regions which lack  
492 geochronological control (for example in the North Sea, Figure 8). These uncertainties, a product of spatial  
493 interpolation across regions with sparse information, are much greater than those associated with individual  
494 dates. Figure 9A shows examples of output maps from ATAT which display the spatial pattern of agreement  
495 and the magnitude of the difference between Experiment C and the DATED reconstruction. This shows that due



496 to the uncertainty associated with North Sea glaciation, even where the model produces an unrealistic artefact,  
497 there is data-model agreement. Furthermore, ATAT produces a map which displays the number of years  
498 between data-based and modelled retreat and/or advance (e.g. Figure 9B). Figure 9B, which compares  
499 Experiment C to the DATED isochrones, shows that the timing of model-data disagreement is spatially variable.  
500 If more modelling simulations were conducted, such maps may reveal regions of reconstruction or particular  
501 dates which are difficult to simulate in the model. In such cases, data or model re-evaluation may be required  
502 and herein lies the potential utility of this ATAT tool in making sense of ensemble model runs. However, such  
503 model-data comparison awaits a full-ensemble simulation which accounts for model uncertainty (e.g. Hubbard  
504 et al., 2009).

## 505 **5. Summary and concluding remarks**

506 Here we present ATAT, an automated timing-accordance tool for comparing ice-sheet model output with  
507 geochronological data and empirical ice sheet reconstructions. We demonstrate the utility of ATAT through  
508 three simplified simulations of the former British-Irish Ice Sheet. Note that a fuller ensemble model of hundreds  
509 to thousands of runs is required for full model evaluation (e.g. Hubbard et al., 2009). ATAT enables users to  
510 quantify the difference between the simulated timing of ice sheet advance and retreat and those from a chosen  
511 dataset, and allows production of cumulative ice coverage agreement maps that should help distinguish between  
512 less and more promising runs. We envisage that this tool will be especially useful for ice-sheet modellers  
513 through justifying model choice from an ensemble, quantifying error and tuning ice-sheet model experiments to  
514 fit data. In the case where locations or regions of data cannot be fit by a model, and all model uncertainty has  
515 been accounted for in an ensemble simulation, the comparisons made in ATAT may also highlight that data re-  
516 evaluation is necessary. ATAT is supplied as supplementary material to this article.

## 517 **6. Code Availability**

518 ATAT 1.0 source code is freely distributed under a GNU GPL licence as supplementary material to this paper  
519 and can be downloaded from <https://figshare.com/s/38d0fd268684ad0fcc2d>. The ice sheet modelling  
520 experiments shown here were conducted using the Parallel Ice Sheet Model (<http://pism-docs.org/>).  
521 Development of PISM is supported by NASA grant NNX17AG65G and NSF grants PLR-1603799 and PLR-  
522 1644277. The geochronological data used is freely available from  
523 <https://www.sciencedirect.com/science/article/pii/S0012825216304408#s0105> and  
524 <https://doi.pangaea.de/10.1594/PANGAEA.848117>.

### 525 **6.1. General Instructions**

526 ATAT is written in python, and distributed as both .py script, for use in Python 2, and a .py3 script, for use with  
527 Python 3. The tool requires installation of Python and the following freely available Python packages:

- 528 • netCDF4 (<https://pypi.python.org/pypi/netCDF4>)
- 529 • numpy (<http://www.numpy.org/>)
- 530 • scipy (<https://www.scipy.org/>)



531       • matplotlib (<https://matplotlib.org/>)  
532       • matplotlib toolkit basemap (<https://matplotlib.org/basemap/>)  
533       ATAT can be run from any Python enabled environment (e.g. IDLE, BASH). Here we provide the  
534 following simple instructions for running ATAT in a BASH shell. Each stage has error reporting.  
535       1. Open a BASH terminal and navigate to the directory containing the ATAT script (e.g. “cd /home/ATAT”).  
536       2. Launch the ATAT script using python (“python ATATv1.0.py”).  
537       3. A command line prompt will ask whether deglacial or advance ages are being tested. Type “DEGLACIAL”  
538 or “ADVANCE” accordingly, and press return.  
539       4. A second prompt will ask for the path to the geochronological data file, type this in and press return (e.g.  
540 “/home/ATAT/geochron.nc”)  
541       5. The user is then asked to specify the path to the ice-sheet model output file (e.g.  
542 “/home/ATAT/icesheetmodel1.nc”)  
543       6. A command line prompt will then ask the user whether the model extent is based on thickness or a mask.  
544 Type THK or MSK accordingly. In the case of MSK, the user is asked to define the numeric value of mask  
545 which represents grounded ice.  
546       7. The user is then asked to define variables related to the output maps. For the model-data offset map (Figure  
547 9B), either RMSE (type “NONE”) or wRMSE (type “WEIGHTED”) can be displayed for each site. For the  
548 cumulative agreement map (Figure 9A), all sites (type “ALL”), those that the model glaciates at some point  
549 (type “COVERED”) or those that agree within error (type “INERROR”) can be displayed.  
550       8. ATAT then prints all statistics for the data-model comparison conducted to a .csv file, default name  
551 “ATAT\_output.csv”.  
552

553 *Acknowledgements:* This work was supported by the Natural Environment Research Council consortium grant;  
554 BRITICE-CHRONO NE/J009768/1.

## 555 **References**

- 556 Applegate, P.J., Kirchner, N., Stone, E.J., Keller, K. and Greve, R. An assessment of key model parametric  
557 uncertainties in projections of Greenland Ice Sheet behavior. *Cryosphere*, 6(3), 589-606, 2012.
- 558 Arnold, J.R. and Libby, W.F. Radiocarbon dates. *Science*, 113(2927), 111-120, 1951.
- 559 Balco, G. Contributions and unrealized potential contributions of cosmogenic-nuclide exposure dating to glacier  
560 chronology, 1990–2010. *Quaternary Sci Rev*, 30(1), 3-27, 2011.
- 561 Bamber, J.L. and Aspinall, W.P.. An expert judgement assessment of future sea level rise from the ice sheets.  
562 *Nat Clim Change*, 3(4), 424-427, 2013.
- 563 Bateman, M.D., Evans, D.J., Roberts, D.H., Medialdea, A., Ely, J. and Clark, C.D., The timing and  
564 consequences of the blockage of the Humber Gap by the last British– Irish Ice Sheet. *Boreas*. 47(1), 41-61,  
565 2018.
- 566 Boulton, G. and Hagdorn, M. Glaciology of the British Isles Ice Sheet during the last glacial cycle: form, flow,  
567 streams and lobes. *Quaternary Sci Rev*, 25(23), 3359-3390, 2006.



- 568 Briggs, R.D. and Tarasov, L. How to evaluate model-derived deglaciation chronologies: a case study using  
569 Antarctica. *Quaternary Sci Rev*, 63, 109-127, 2013.
- 570 Briggs, R.D., Pollard, D. and Tarasov, L. A data-constrained large ensemble analysis of Antarctic evolution  
571 since the Eemian. *Quaternary Sci Rev*, 103, 91-115, 2014.
- 572 Brown, E.J., Rose, J., Coope, R.G. and Lowe, J.J. An MIS 3 age organic deposit from Balglass Burn, central  
573 Scotland: palaeoenvironmental significance and implications for the timing of the onset of the LGM ice sheet in  
574 the vicinity of the British Isles. *J Quaternary Sci*, 22(3), 295-308, 2007.
- 575 Bueler, E.D., Lingle, C.S. and Brown, J. Fast computation of a viscoelastic deformable Earth model for ice-  
576 sheet simulations. *Ann Glaciol*, 46(1), 97-105, 2007.
- 577 Bueler, E. and Brown, J. Shallow shelf approximation as a “sliding law” in a thermomechanically coupled ice  
578 sheet model. *J Geophys Res-Earth*, 114(F3), 2009.
- 579 Calov, R. and Greve, R. A semi-analytical solution for the positive degree-day model with stochastic  
580 temperature variations. *J Glaciol*, 51(172), 173-175, 2005.
- 581 Chiverrell, R.C., Thrasher, I.M., Thomas, G.S., Lang, A., Scourse, J.D., van Landeghem, K.J., Mccarroll, D.,  
582 Clark, C.D., Cofaigh, C.Ó., Evans, D.J. and Ballantyne, C.K. Bayesian modelling the retreat of the Irish Sea Ice  
583 Stream. *J Quaternary Sci*, 28(2), 200-209, 2013.
- 584 Clark, C.D., Hughes, A.L., Greenwood, S.L., Jordan, C. and Sejrup, H.P. Pattern and timing of retreat of the last  
585 British-Irish Ice Sheet. *Quaternary Sci Rev*, 44, 112-146, 2012.
- 586 Cornford, S.L., Martin, D.F., Graves, D.T., Ranken, D.F., Le Brocq, A.M., Gladstone, R.M., Payne, A.J., Ng,  
587 E.G. and Lipscomb, W.H. Adaptive mesh, finite volume modeling of marine ice sheets. *Journal of*  
588 *Computational Physics*, 232(1), 529-549, 2013.
- 589 DeConto, R.M. and Pollard, D. Contribution of Antarctica to past and future sea-level rise. *Nature*, 531(7596),  
590 591-597, 2016.
- 591 Duller, G.A.T. Single grain optical dating of glacial deposits. *Quaternary Geochronology*, 1(4), 296-304,  
592 2006.
- 593 Dyke, A.S. An outline of North American deglaciation with emphasis on central and northern Canada.  
594 *Developments in Quaternary Sciences*, 2, 373-424, 2004.
- 595 Dyke, A.S. An outline of North American deglaciation with emphasis on central and northern Canada.  
596 *Developments in Quaternary Sciences*, 2, 373-424, 2004.
- 597 Edwards, T.L., Fettweis, X., Gagliardini, O., Gillet-Chaulet, F., Goelzer, H., Gregory, J.M., Hoffman, M.,  
598 Huybrechts, P., Payne, A.J., Perego, M. and Price, S. Effect of uncertainty in surface mass balance-elevation  
599 feedback on projections of the future sea level contribution of the Greenland ice sheet. *Cryosphere*, 8(1), 195-  
600 208. 2014.
- 601 Fowler, A.C. A sliding law for glaciers of constant viscosity in the presence of subglacial cavitation. In  
602 *Proceedings of the Royal Society of London A: Mathematical, Physical and Engineering Sciences*, 407(1832),  
603 147-170, 1986.
- 604 Fretwell, P., Pritchard, H.D., Vaughan, D., Bamber, J.L., Barrand, N.E., Bell, R., Bianchi, C., Bingham, R.G.,  
605 Blankenship, D.D., Casassa, G. and Catania, G. Bedmap2: improved ice bed, surface and thickness datasets for  
606 Antarctica. *Cryosphere*, 7, 375-393, 2013.





- 607 Fuchs, M. and Owen, L.A. Luminescence dating of glacial and associated sediments: review, recommendations  
608 and future directions. *Boreas*, 37(4), 636-659, 2008.
- 609 Gasson, E., DeConto, R.M., Pollard, D. and Levy, R.H. Dynamic Antarctic ice sheet during the early to mid-  
610 Miocene. *Proceedings of the National Academy of Sciences*, 113(13), 3459-3464, 2016.
- 611 Golledge, N.R., Levy, R.H., McKay, R.M., Fogwill, C.J., White, D.A., Graham, A.G., Smith, J.A., Hillenbrand,  
612 C.D., Licht, K.J., Denton, G.H. and Ackert, R.P. Glaciology and geological signature of the Last Glacial  
613 Maximum Antarctic ice sheet. *Quaternary Sci Rev*, 78, 225-247, 2013.
- 614 Gomez, N., Pollard, D., Mitrovica, J.X., Huybers, P., Clark, P.U. Evolution of a coupled marine ice sheet-sea  
615 level model, *J Geophys Res*, 117, F01013, 2012.
- 616 Gomez, N., Pollard, D. and Mitrovica, J.X. A 3-D coupled ice sheet–sea level model applied to Antarctica  
617 through the last 40 ky. *Earth and Planet Sc Lett*, 384, 88-99, 2013.
- 618 Gowan, E.J. An assessment of the minimum timing of ice free conditions of the western Laurentide Ice Sheet.  
619 *Quaternary Sci Rev*, 75, 100-113, 2013.
- 620 Gregoire, L.J., Payne, A.J. and Valdes, P.J. Deglacial rapid sea level rises caused by ice-sheet saddle collapses.  
621 *Nature*, 487(7406), 219-222, 2012.
- 622 Greve, R. and Hutter, K. Polythermal three-dimensional modelling of the Greenland ice sheet with varied  
623 geothermal heat flux. *Ann Glaciol*, 21, 8-12, 1995.
- 624 Gudmundsson, G.H., Krug, J., Durand, G., Favier, L. and Gagliardini, O. The stability of grounding lines on  
625 retrograde slopes. *Cryosphere*, 6, 1497-1505, 2012.
- 626 Gudmundsson, G.H. Ice-shelf buttressing and the stability of marine ice sheets, *Cryosphere*, 7, 647-655, 2013.
- 627 Heroy, D.C. and Anderson, J.B. Radiocarbon constraints on Antarctic Peninsula ice sheet retreat following the  
628 Last Glacial Maximum (LGM). *Quaternary Sci Rev*, 26(25), 3286-3297, 2007.
- 629 Heyman, J., Stroeven, A.P., Harbor, J.M. and Caffee, M.W. Too young or too old: evaluating cosmogenic  
630 exposure dating based on an analysis of compiled boulder exposure ages. *Earth Planet Sc Lett*, 302(1), 71-80,  
631 2011.
- 632 Hindmarsh, R.C. Consistent generation of ice-streams via thermo-viscous instabilities modulated by membrane  
633 stresses. *Geophys Res Lett*, 36(6). 2009.
- 634 Hubbard, A., Bradwell, T., Golledge, N., Hall, A., Patton, H., Sugden, D., Cooper, R. and Stoker, M. Dynamic  
635 cycles, ice streams and their impact on the extent, chronology and deglaciation of the British–Irish ice sheet.  
636 *Quaternary Sci Rev*, 28(7), 758-776, 2009.
- 637 Hughes, A.L., Greenwood, S.L. and Clark, C.D. Dating constraints on the last British-Irish Ice Sheet: a map and  
638 database. *J Maps*, 7(1), 156-184, 2011.
- 639 Hughes, A.L., Clark, C.D. and Jordan, C.J. Flow-pattern evolution of the last British Ice Sheet. *Quaternary Sci*  
640 *Rev*, 89, 148-168, 2014.
- 641 Hughes, A.L., Gyllencreutz, R., Lohne, Ø.S., Mangerud, J. and Svendsen, J.I. The last Eurasian ice sheets—a  
642 chronological database and time-slice reconstruction, DATED-1. *Boreas*, 45(1), 1-45, 2016.
- 643 Hughes, T.J., Is the West Antarctic ice sheet disintegrating? *J. Geophys. Res.*, 78 (33), 7884-7910, 1973.
- 644 Imbrie, J., Hays, J.D., Martinson, D.G., McIntyre, A., Mix, A.C., Morley, J.J., Pisias, N.G., Prell, W.L.,  
645 Shackleton, N.J. The orbital theory of Pleistocene climate: support from a revised chronology of the marine



- 646  $\delta^{18}O$  record. In: Berger, A., Imbrie, J., Hays, H., Kukla, G., Saltzman, B. (Eds.), *Milankovitch and Climate*,  
647 Part I. D. Reidel Publishing, Dordrecht, 269–305, 1984.
- 648 Johnsen, S.J., Dahl-Jensen, D., Dansgaard, W. and Gundestrup, N. Greenland palaeotemperatures derived from  
649 GRIP bore hole temperature and ice core isotope profiles. *Tellus B*, 47(5), 624–629, 1995.
- 650 Kirchner, N., Hutter, K., Jakobsson, M. and Gyllencreutz, R. Capabilities and limitations of numerical ice sheet  
651 models: a discussion for Earth-scientists and modelers. *Quaternary Sci Rev*, 30(25), 3691–3704, 2011.
- 652 Kirchner, N., Ahlkrone, J., Gowan, E.J., Lötstedt, P., Lea, J.M., Noormets, R., von Sydow, L., Dowdeswell, J.A.  
653 and Benham, T. Shallow ice approximation, second order shallow ice approximation, and full Stokes models: A  
654 discussion of their roles in palaeo-ice sheet modelling and development. *Quaternary Sci Rev*, 147, 136–147,  
655 2016.
- 656 Kleman, J., Hättestrand, C., Stroeven, A.P., Jansson, K.N., De Angelis, H. and Borgström, I. Reconstruction of  
657 Palaeo-Ice Sheets-Inversion of their Glacial Geomorphological Record. In Knight, P.G. (Eds) *Glacier science*  
658 *and environmental change, 192–198*, 2006.
- 659 Larour, E., Seroussi, H., Morlighem, M. and Rignot, E. Continental scale, high order, high spatial resolution, ice  
660 sheet modeling using the Ice Sheet System Model (ISSM). *J Geophys Res-Earth*, 117(F1), 2012.
- 661 Libby, W.F., Anderson, E.C. and Arnold, J.R. Age determination by radiocarbon content: world-wide assay of  
662 natural radiocarbon. *Science*, 109(2827), 227–228, 1949.
- 663 Lingle, C.S. and Clark, J.A. A numerical model of interactions between a marine ice sheet and the solid earth:  
664 Application to a West Antarctic ice stream. *J Geophys Res-Oceans*, 90(C1), 1100–1114, 1985.
- 665 Livingstone, S.J., Cofaigh, C.Ó., Stokes, C.R., Hillenbrand, C.D., Vieli, A. and Jamieson, S.S. Antarctic palaeo-  
666 ice streams. *Earth-Sci Rev*, 111(1), 90–128, 2012.
- 667 Lorenz, E.N. Deterministic Nonperiodic Flow, *J. Atmos. Sci.*, 20, 130–141, 1963.
- 668 Lowe, J.J. and Walker, M.J. Radiocarbon Dating the Last Glacial-Interglacial Transition (Ca. 14–9 14C Ka Bp)  
669 in Terrestrial and Marine Records: The Need for New Quality Assurance Protocols. *Radiocarbon*, 42(1), 53–68,  
670 2000.
- 671 Lowell, T.V., Fisher, T.G., Hajdas, I., Glover, K., Loope, H. and Henry, T. Radiocarbon deglaciation  
672 chronology of the Thunder Bay, Ontario area and implications for ice sheet retreat patterns. *Quaternary Sci Rev*,  
673 28(17), 1597–1607, 2009.
- 674 Lukas, S., Spencer, J.Q., Robinson, R.A. and Benn, D.I. Problems associated with luminescence dating of Late  
675 Quaternary glacial sediments in the NW Scottish Highlands. *Quaternary Geochron*, 2(1), 243–248, 2007.
- 676 Mercer, J.H. West Antarctic ice sheet and CO<sub>2</sub> greenhouse effect: a threat of disaster. *Nature*, 271, 321–325,  
677 1978.
- 678 Napieralski, J., Harbor, J. and Li, Y. Glacial geomorphology and geographic information systems. *Earth-Sci*  
679 *Rev*, 85(1), 1–22, 2007.
- 680 Ó Cofaigh, C.Ó. and Evans, D.J. Radiocarbon constraints on the age of the maximum advance of the British–  
681 Irish Ice Sheet in the Celtic Sea. *Quaternary Sci Rev*, 26(9), 1197–1203, 2007.
- 682 Patton, H., Hubbard, A., Andreassen, K., Winsborrow, M. and Stroeven, A.P. The build-up, configuration, and  
683 dynamical sensitivity of the Eurasian ice-sheet complex to Late Weichselian climatic and oceanic forcing.  
684 *Quaternary Sci Rev*, 153, 97–121, 2016.



- 685 Pattyn, F. Sea-level response to melting of Antarctic ice shelves on multi-centennial timescales with the fast  
686 Elementary Thermomechanical Ice Sheet model (f. ETISH v1. 0). *Cryosphere*, 11(4), p.1851-1878, 2017.
- 687 Pattyn, F., Perichon, L., Aschwanden, A., Breuer, B., De Smedt, B., Gagliardini, O., Gudmundsson, G.H.,  
688 Hindmarsh, R., Hubbard, A., Johnson, J.V. and Kleiner, T. Benchmark experiments for higher-order and full  
689 Stokes ice sheet models (ISMIP-HOM). *Cryosphere*, 2(1), 111-151, 2008.
- 690 Pattyn, F., Schoof, C., Perichon, L., Hindmarsh, R.C.A., Bueler, E., Fleurian, B.D., Durand, G., Gagliardini, O.,  
691 Gladstone, R., Goldberg, D. and Gudmundsson, G.H. Results of the marine ice sheet model intercomparison  
692 project, MISIP. *Cryosphere*, 6(3), 573-588, 2012.
- 693 Pollard, D. and DeConto, R.M. Modelling West Antarctic ice sheet growth and collapse through the past five  
694 million years. *Nature*, 458(7236), 329-332, 2009.
- 695 Ritz, C., Edwards, T.L., Durand, G., Payne, A.J., Peyaud, V. and Hindmarsh, R.C. Potential sea-level rise from  
696 Antarctic ice-sheet instability constrained by observations. *Nature*, 528(7580), 115-118, 2015.
- 697 Robinson, A., Calov, R. and Ganopolski, A. Greenland ice sheet model parameters constrained using  
698 simulations of the Eemian Interglacial. *Clim Past*, 7(2), 381-396, 2011.
- 699 Rutt, I.C., Hagdorn, M., Hulton, N.R.J. and Payne, A.J. The Glimmer community ice sheet model. *J Geophys*  
700 *Res-Earth*, 114(F2), 2009.
- 701 Schoof, C.S. Ice sheet grounding line dynamics: steady states, stability and hysteresis. *J. Geophys. Res. Earth*  
702 *Surf.*, 112, F03S28, 2007.
- 703 Schoof, C. Coulomb friction and other sliding laws in a higher-order glacier flow model. *Math Mod Meth Appl*  
704 *S*, 20(01), 157-189, 2010.
- 705 Schoof, C. Marine ice sheet stability. *J. Fluid Mech.*, 698, 62-72, 2012.
- 706 Seddik, H., Greve, R., Zwinger, T., Gillet-Chaulet, F. and Gagliardini, O. Simulations of the Greenland ice sheet  
707 100 years into the future with the full Stokes model Elmer/Ice. *J Glaciol*, 58(209), 427-440, 2012.
- 708 Seguinot, J., Rogozhina, I., Stroeven, A.P., Margold, M. and Kleman, J. Numerical simulations of the  
709 Cordilleran ice sheet through the last glacial cycle. *Cryosphere*, 10, 639-664, 2016.
- 710 Simpson, M.J., Milne, G.A., Huybrechts, P. and Long, A.J. Calibrating a glaciological model of the Greenland  
711 ice sheet from the Last Glacial Maximum to present-day using field observations of relative sea level and ice  
712 extent. *Quaternary Sci Rev*, 28(17), 1631-1657, 2009.
- 713 Small, D., Clark, C.D., Chiverrell, R.C., Smedley, R.K., Bateman, M.D., Duller, G.A., Ely, J.C., Fabel, D.,  
714 Medialdea, A. and Moreton, S.G. Devising quality assurance procedures for assessment of legacy  
715 geochronological data relating to deglaciation of the last British-Irish Ice Sheet. *Earth-Sci Rev*, 164, 232-250,  
716 2017.
- 717 Smedley, R.K., Glasser, N.F. and Duller, G.A.T. Luminescence dating of glacial advances at Lago Buenos Aires  
718 (~ 46° S), Patagonia. *Quaternary Sci Rev*, 134, 59-73, 2016.
- 719 Smedley, R.K., Chiverrell, R.C., Ballantyne, C.K., Burke, M.J., Clark, C.D., Duller, G.A.T., Fabel, D.,  
720 McCarroll, D., Scourse, J.D., Small, D. and Thomas, G.S.P. Internal dynamics condition centennial-scale  
721 oscillations in marine-based ice-stream retreat. *Geology*, 45(9), 787-790, 2017.
- 722 Stokes, C.R., Tarasov, L., Blomdin, R., Cronin, T.M., Fisher, T.G., Gyllencreutz, R., Hättestrand, C., Heyman,  
723 J., Hindmarsh, R.C., Hughes, A.L. and Jakobsson, M. On the reconstruction of palaeo-ice sheets: recent  
724 advances and future challenges. *Quaternary Sci Rev*, 125, 15-49, 2015.



725 Tarasov, L. and Peltier, W.R. A geophysically constrained large ensemble analysis of the deglacial history of the  
 726 North American ice-sheet complex. *Quaternary Sci Rev*, 23(3), 359-388, 2004.  
 727 Tarasov, L., Dyke, A.S., Neal, R.M. and Peltier, W.R. A data-calibrated distribution of deglacial chronologies  
 728 for the North American ice complex from glaciological modeling. *Earth Planet Sc Lett*, 315, 30-40, 2012.  
 729 Tushingham, A.M. and Peltier, W.R. Validation of the ICE-3G Model of Würm-Wisconsin Deglaciation using a  
 730 global data base of relative sea level histories. *J Geophys Res-Solid Earth*, 97(B3), 3285-3304, 1992.  
 731 Weertman, J. Stability of the junction of an ice-sheet and an ice-shelf. *J. Glaciol.* 13 (67), 3-11), 1974.  
 732 Winkelmann, R., Martin, M.A., Haseloff, M., Albrecht, T., Bueller, E., Khroulev, C. and Levermann, A. The  
 733 Potsdam parallel ice sheet model (PISM-PIK)-Part 1: Model description. *Cryosphere*, 5(3), 715-726, 2011.  
 734

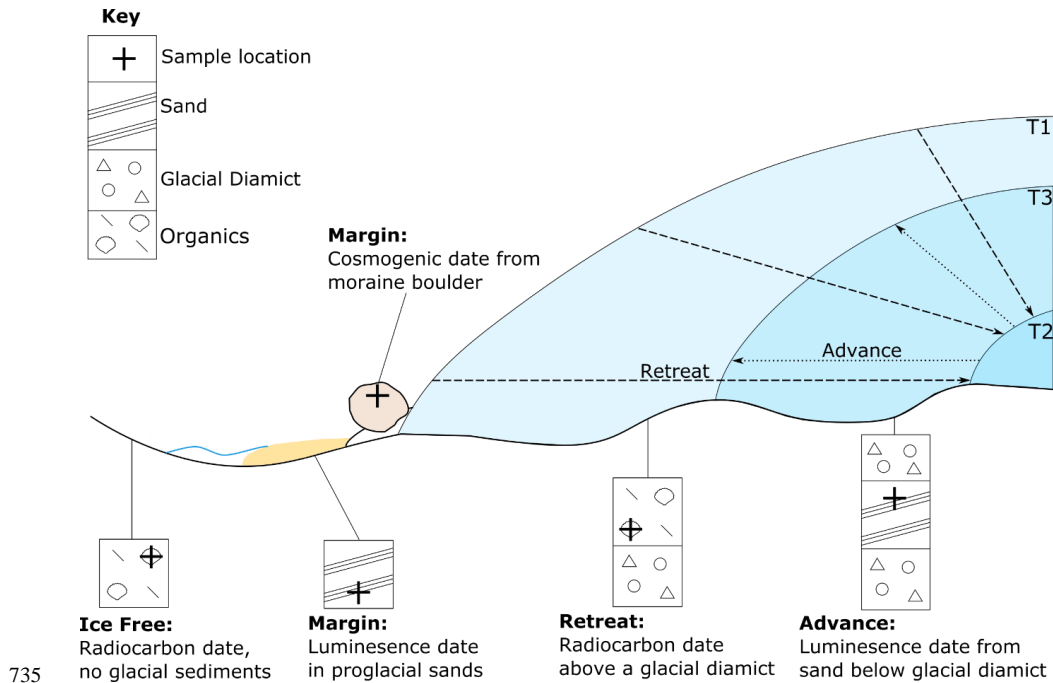
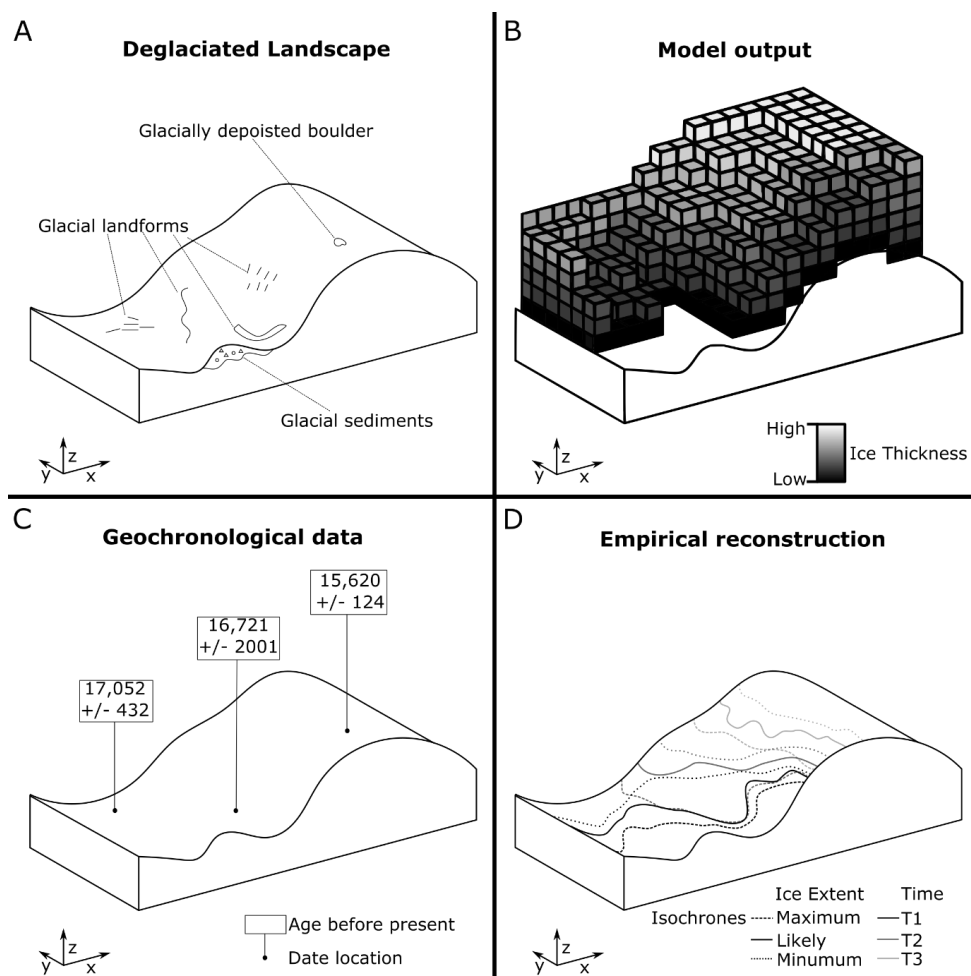


Figure 1: Schematic illustration of stratigraphic and inferred glaciological context of geochronological data. Note that at T1 the ice sheet is at its most advanced. It then retreats to a minimum at T2, before re-advancing to T3.



738

739

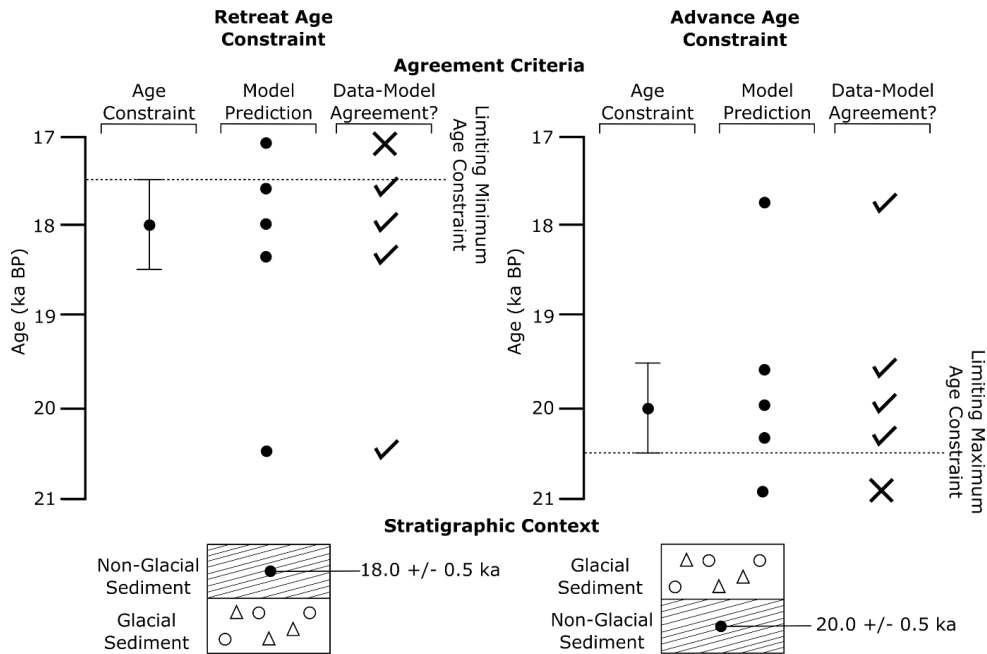
740

741

742

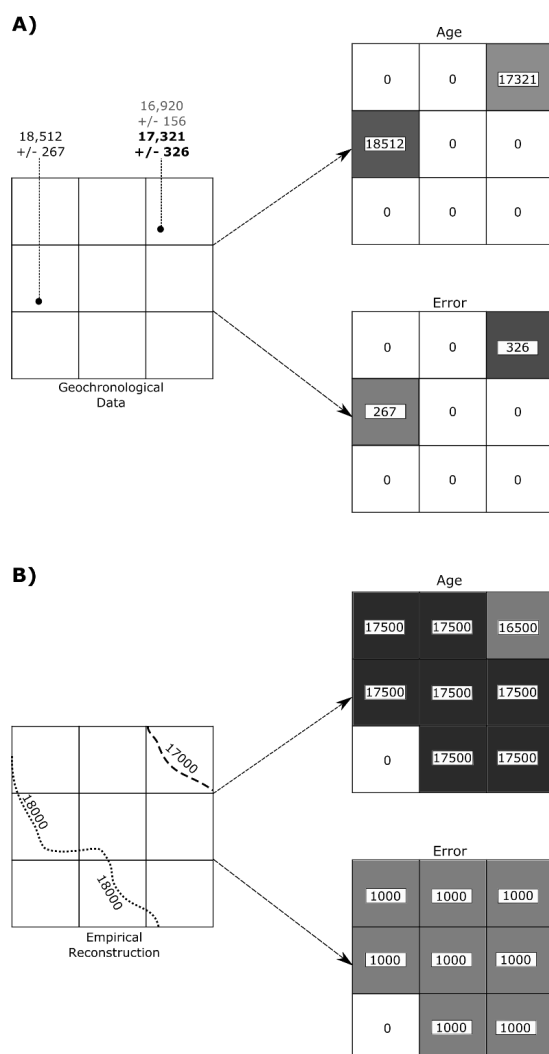
743

**Figure 2.** Schematic of geochronological data and ice-sheet model output. A) A deglaciated landscape, demonstrating some of the features used by palaeo-glaciologists when empirically reconstructing an ice sheet. B) Ice-sheet model output, displaying modelled ice-sheet thickness, in this case at a specific time. C) Geochronological data. D) Empirical reconstruction. Note how the nature of these data vary between source.



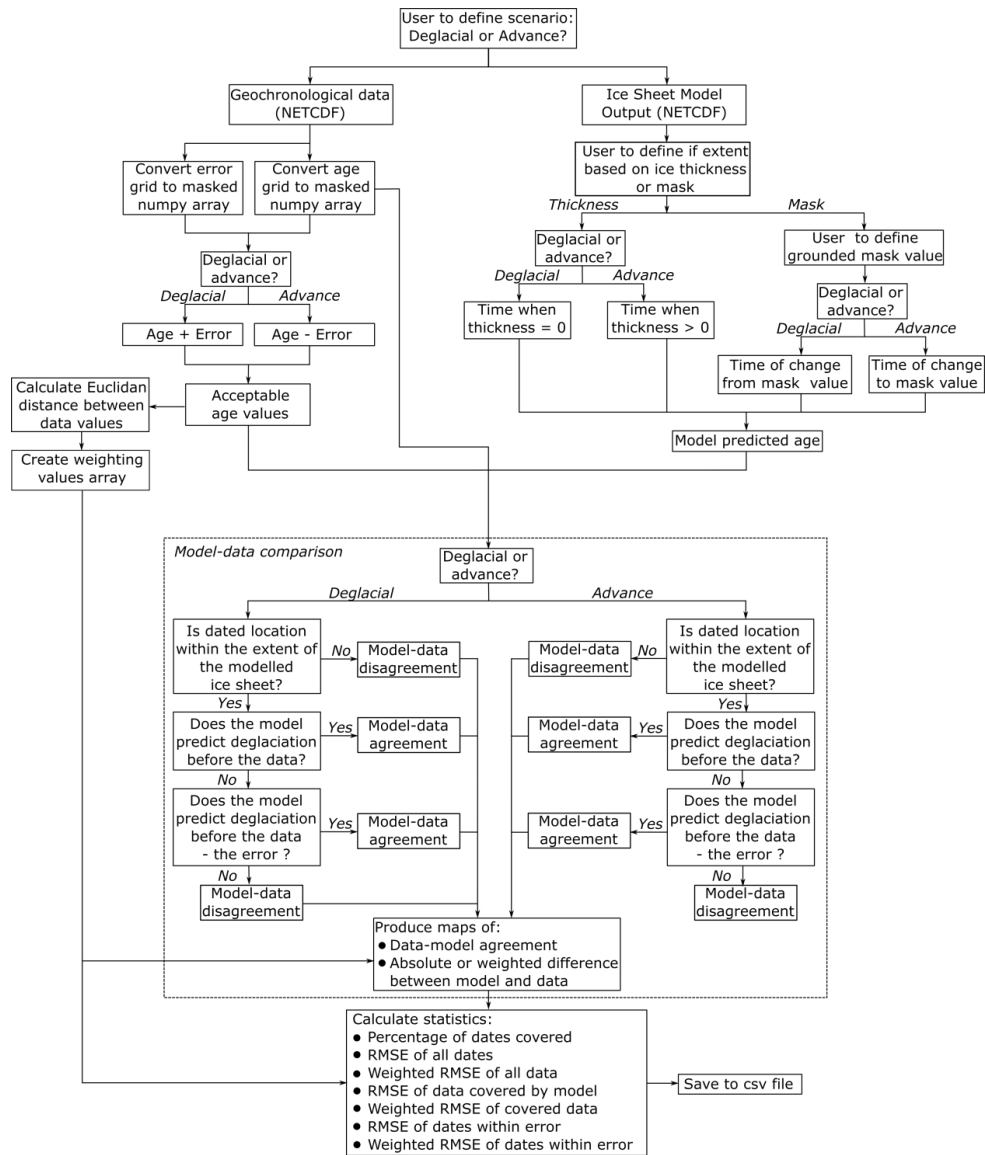
744

745 **Figure 3. Identification of data-model agreement with consideration of error by ATAT for retreat (left)**  
 746 **and advance (right) data. If a model predicts ice free conditions before an ice-free age, or during the**  
 747 **associated error, there is data-model agreement. If deglaciation occurs at this location after the error, the**  
 748 **model disagrees with the data. If a model predicts ice advance and cover before the advance age and its**  
 749 **associated error, there is model-data disagreement. Agreement between the model and data occurs if ice**  
 750 **advances over the location after the date, or before the date within the range of the error.**



751

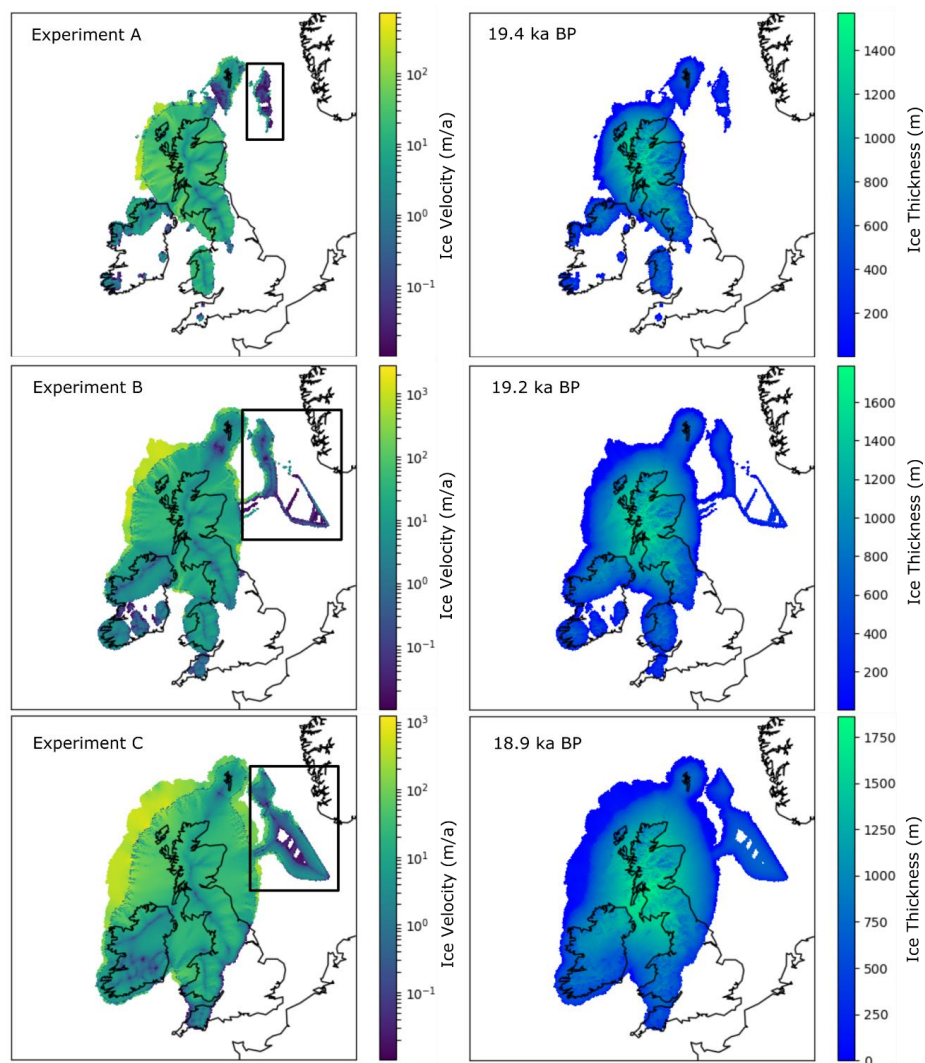
752 **Figure 4. Examples of empirical data preparation for ATAT. (A) Conversion of geochronological data**  
 753 **into a grid for ATAT. In this example the user has made a judgement based on a priori knowledge that**  
 754 **the date of  $17,321 \pm 326$  is most representative of the event of interest. Note that age and error are split**  
 755 **into separate grids, and that no data regions are assigned a value of 0. (B) Conversion of an empirical**  
 756 **reconstruction (margin isochrones) into a grid for ATAT. Here we simply assume that the area between**  
 757 **isochrones became deglaciated between at the age between the two isochrones, and that associated error**  
 758 **is 1000 years. More complex reconstructions (e.g. Hughes et al., 2016) may require different user-defined**  
 759 **rules.**



760

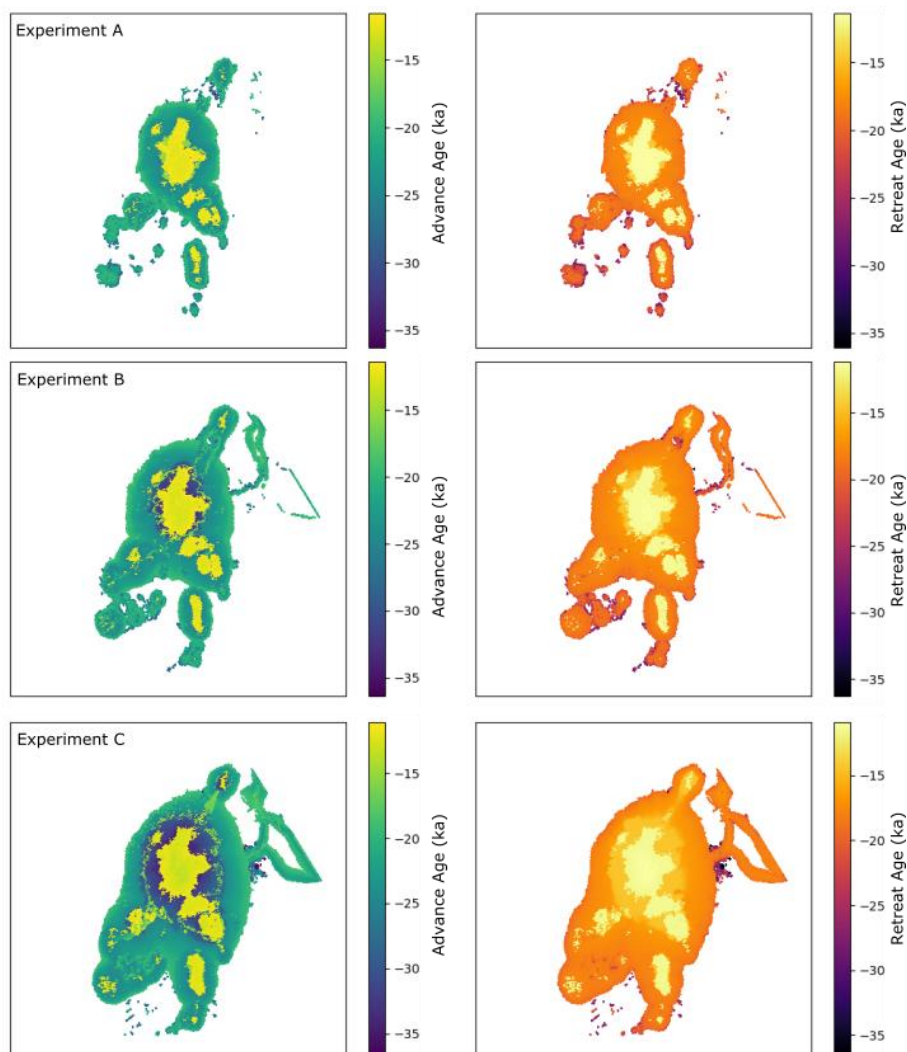
761 **Figure 5. Flow chart of ATAT procedure. See text for further description.**





762

763 **Figure 6.** Maximum extent of produced ice sheet for the three experiments. Experiment B is 1°C colder  
 764 than A, and experiment C is 2°C colder than A. Left panel shows ice velocity, right is ice thickness. The  
 765 box on the left panel highlights likely erroneous output in the North Sea, likely a consequence of model  
 766 domain, discussed further in the text.

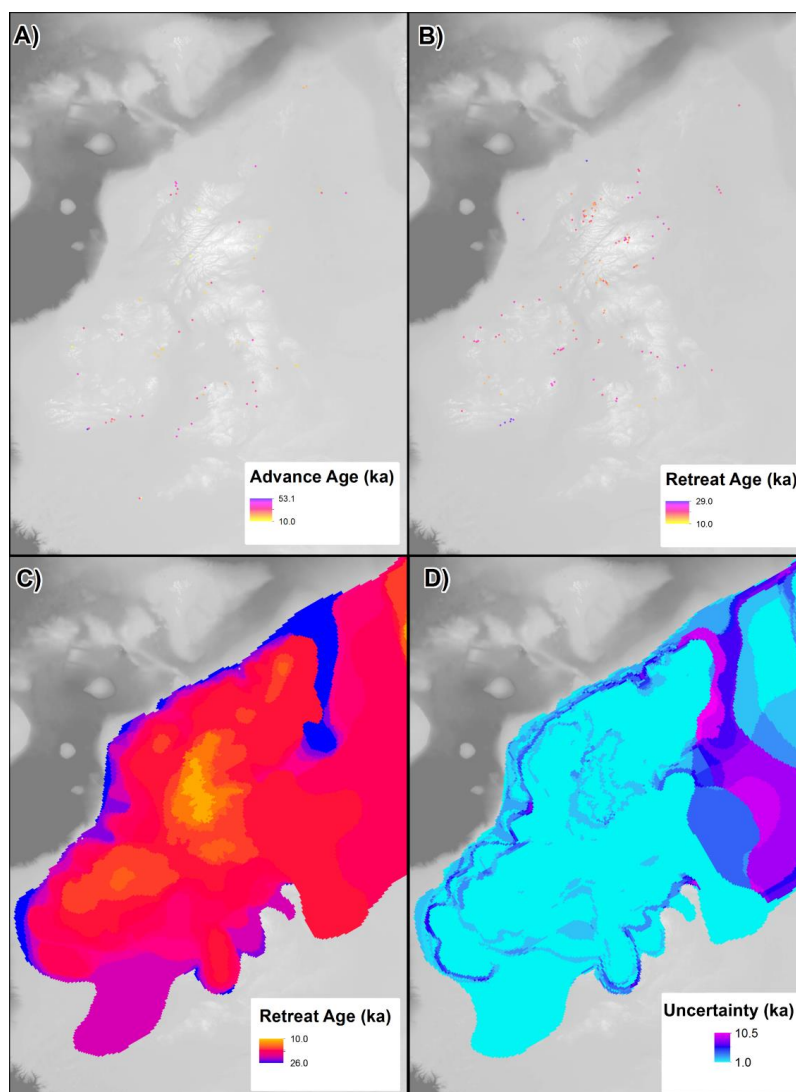


767

768 **Figure 7. Timing of advance (left) and retreat (right) from the three ice sheet modelling experiments.**

769 **Experiments are the same as in Figure 6. The early ages toward the centre of the model, and centred over**

770 **higher topography, represent the modelled extent of the Younger Dryas readvance.**



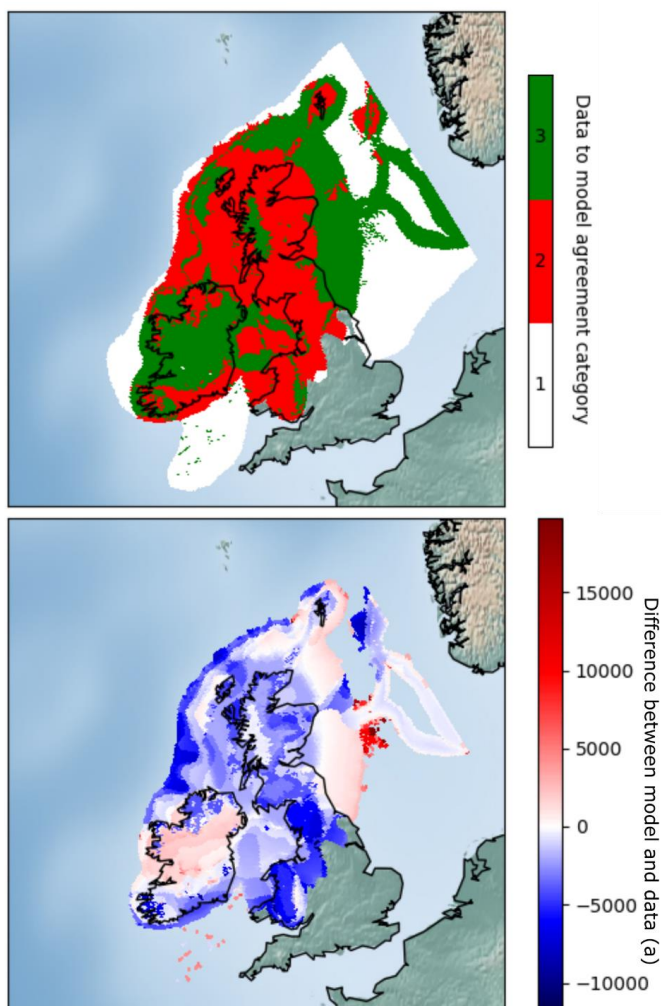
771

772 **Figure 8.** Example of geochronological data projected onto model raster grids; as point-data in A and B

773 and from an empirical reconstruction in C and D. (A). Advance ages from Hughes et al. (2016). (B)

774 Retreat ages from Small et al. (2017). (C) Retreat age derived from DATED isochrone reconstruction

775 (Hughes et al., 2016). (D) Error associated with reconstruction in C.



776

777 **Figure 9.** Example mapped outputs from ATAT. In this case, experiment C was compared with the  
778 **DATED** reconstruction. Top map (cumulative agreement) shows categories of data-model agreement  
779 across the domain, where 1 = not covered by model, 2 = no agreement and 3 = data-model agreement  
780 within error. The lower map (model-data offset) shows magnitude of difference between model and data;  
781 negative values show a modelled retreat of ice later than the **DATED** isochrones, and positive values show  
782 a modelled retreat of ice before the **DATED** isochrones.



783 Table 1. Classification of geochronological data (after Hughes et al., 2011) and its use in ATAT.

<b>Class</b>	<b>Glaciological context</b>	<b>Stratigraphic context</b>	<b>Example</b>	<b>Use in ATAT</b>
Advance	Ice-sheet build up	Material directly below or incorporated within glacial diamict	Luminescence date from a sand below a glacial diamict	Ice cover a short time after this date
Retreat	Ice-free after ice cover	Dated material above glacial diamict	Radiocarbon date of a shell above a glacial diamict	Ice-free conditions from this date onwards (note deglaciation could have occurred a long time before)
Ice Free	Ice-free, but lacking direct information regarding ice	Dated material which indicates ice-free conditions but has no relation to ice cover. It may be much younger and not provide much useful constraint.	Radiocarbon date of organic sediments without underlying glacial sediments	
Margin	Proximal to an ice sheet margin	Dated material with information that ties it to an ice margin	Luminescence date in proglacial sands	
Exposure time (cumulative)	Length of time since sample exposed	N/A	Cosmogenic isotope on erratic boulder above a trimline	Not used

784



Table 2. Comparison of attributes between geochronological data and ice sheet model output.

	<b>Nature of data produced</b>	<b>Spatial resolution</b>	<b>Spatial continuity</b>	<b>Temporal frequency and resolution</b>	<b>Sources of uncertainty</b>	<b>Main limitation</b>
<b>Geochronological data</b>	Timing of the absence of ice at a location	Point location	Point location, unevenly distributed in space, but can be interpolated	Determined by data availability and associated error	Instrumental, environmental and stratigraphic factors	Reliant upon correct stratigraphic interpretation to tie to glaciological events
<b>Ice-sheet model output</b>	Simulation of physically plausible ice sheet conditions	Various, ranging from tens to unit kilometres.	Spatially even, regularly-spaced across entire domain	Continuous in time. Precise subannual resolution possible, but not recorded in practice	Parameterisations, boundary conditions	Based upon mathematical and physical approximations of ice flow



Table 3. Required input variables for ATAT NetCDF files.

Data source	NetCDF Variable	Units	Dimensions	Description	Notes
	Time	Years before present	x, y	Calendar years before present	
<b>Ice sheet model output</b>	thk	m	time, x,y	Ice thickness	Either “thk” or “msk” required by ATAT.
	msk	Integers	time, x,y	Grounded/floating/icefree mask	Either “thk” or “msk” required by ATAT. User defines value referring to the location of grounded ice
<b>Both</b>	lat	Decimal degrees	x, y	Latitude	
	lon	Decimal degrees	x, y	Longitude	
<b>Geochronological data</b>	age	Years before present	x, y	Timing of deglaciated conditions	Deglacial and advance ages must be in separate files.
	error	Years	x, y	Error associated with deglaciated conditions	Error associated with either deglacial and advance age must be in associated separate file.